

SIMULATED DOPPLER VELOCITY SIGNATURES OF EVOLVING TORNADO-LIKE VORTICES

Robert Davies-Jones* and Vincent T. Wood
National Severe Storms Laboratory, NOAA
Norman, Oklahoma

1. INTRODUCTION

Azimuthal resolution of a vortex depends on the aspect ratio (AR), defined as the ratio of the radar's effective beamwidth to the vortex's core radius (Burgess et al. 1993). For a mesocyclone, tornado cyclone, or a large tornado close to the radar, the aspect ratio may be smaller than one. In this case, the vortex is resolved and has a mesocyclone, tornado-cyclone, or tornado signature (Burgess et al. 1993, 2002; Brown 1998; Brown et al. 2002). As the vortex contracts, its core becomes inadequately resolved and its signature becomes a TVS at $AR = 2$. Tornado warnings are based partially on detection of a tornadic vortex signature (TVS) by a Weather Surveillance Radar-88 Doppler (WSR-88D). This detection depends on tornado strength and core radius, and on the size of the radar sampling volume. Based on variations in damage severity along tornado paths, Burgess et al. (2002) and Wakimoto et al. (2003) concluded that TVS strength was a poor measure of tornado intensity.

Meteorologists and automated algorithms measure the strength of a convergent vortex by the velocity difference (ΔV or ΔV) between the two peaks in the characteristic velocity couplet (e.g., Mitchell et al. 1998; Stumpf et al. 1998). The rotational velocity V_{rot} is $\Delta V/2$. The shear is also used. It is given by $S_D \equiv \Delta V/D$ where D is the distance between the peaks.

Researchers have learned much about how Doppler-velocity signatures of mesocyclones and tornadoes vary with core size and azimuthal resolution by using a WSR-88D computer simulator to

produce signatures of theoretical Rankine combined vortices (Wood and Brown 1992, 1997; Wood et al. 2001; Brown et al. 2002). The idealized vortices in these simulations are steady and inviscid. The peak in the tangential velocity profile is a cusp, which would be rounded off and reduced by diffusion in a real flow.

In this paper we use unsteady versions of the inviscid Rankine combined and the viscous Burgers-Rott vortices. These are exact solutions of the governing equations for neutrally stratified incompressible flow that we have placed in convenient form for Doppler-radar applications (section 2). The vortices initially are tornado cyclones (core diameters of 2 km) and contract to tornadoes as a result of vertical stretching in uniformly convergent flow. This is tornadogenesis without a dynamic pipe effect (Trapp and Davies-Jones 1997). These types of tornadoes form rapidly and simultaneously over a depth spanning the lowest few kilometers with little advance warning unless the warning is based on detection of increasing convergence beneath a mesocyclone aloft (Burgess 2004). In contrast, tornadoes that form with a dynamic pipe effect descend from aloft and develop more slowly, allowing the issuance of warnings with long lead times based on TVS detection. We perform experiments with different values of the constant eddy viscosity and the uniform convergence (section 3) to obtain tornadoes of different intensities, sizes, formation rates and decay rates. In section 4 we use a new simulator to investigate how signature parameters change during tornadogenesis as a tornado-cyclone signature appears and evolves into a TVS. Finally, in section 5 we show that the circulation of the Doppler-velocity signature varies much less than other parameters during vortex evolution, and thus may be a useful advance indicator of tornado threat as long as the flow is convergent.

2. ANALYTICAL REPRESENTATION OF TORNADO-LIKE VORTICES

*Corresponding author address: Robert Davies-Jones, National Severe Storms Laboratory, NOAA, 1313 Halley Circle, Norman, Oklahoma 73069-8493.
e-mail: Bob.Davies-Jones@noaa.gov

To represent tornado-like vortices in our study, we use exact unsteady vortex solutions of the Navier-Stokes or Euler equations of motion and the incompressible continuity equation. We will refer often to their steady counterparts so we briefly review steady exact solutions.

a. Steady vortex solutions

A classic model of inviscid vortex flow is the idealized, steady-state Rankine (1901) combined vortex (henceforth RCV), which consists of an inner core of solid-body rotation and an outer region where the flow is the same as a potential vortex. Within the solidly rotating core, tangential velocity v is directly proportional to radial distance r from the center of the vortex (i.e., $v \propto r$). The maximum tangential velocity occurs at the core wall (outer edge of the core) where there is a cusp in the radial profile of tangential velocity. Beyond the core radius, the tangential velocity decreases as r^{-1} and the circulation, $\Gamma \equiv 2\pi vr$, is constant. The steady RCV has no through flow (i.e., motions in the radial and axial directions).

The viscous steady-state Burgers (1948)-Rott (1958) vortex (henceforth BRV) is a more realistic model than the RCV. The BRV is a one-celled vortex model in which fluid spirals in toward the z -axis as it rises. Instead of the RCV's cusp in the tangential velocity profile, the BRV has a smooth rounded maximum at the radius of maximum tangential winds (the core radius), owing to the constant eddy viscosity ν_e . There is a balance between inward advection and outward diffusion of angular momentum.

b. Time-dependent vortex solutions

In this paper we use unsteady versions of the RCV and BRV (Rott 1958) to investigate the signatures of developing tornado-like vortices. Since the flows are axisymmetric and uniformly convergent, all the solutions have the same radial and vertical velocities,

$$\begin{aligned} dr/dt &\equiv u = -ar \\ dz/dt &\equiv w = 2az, \end{aligned} \quad (1)$$

where $2a$ is the horizontal convergence.

The tangential velocity of the unsteady RCV is

$$v(r,t) = \begin{cases} v_m(t)r/r_c(t), & r \leq r_c(t) \\ v_m(t)r_c(t)/r, & r \geq r_c(t) \end{cases} \quad (2)$$

where $v_m(t)$ is the maximum tangential velocity at time t and the core radius $r_c(t)$ is related to the initial core radius (at $t = t_0$) by

$$r_c(t) = r_c(t_0) \exp[-a(t - t_0)], \quad (3)$$

as illustrated in Fig. 1a. In the absence of diffusion the core wall is a material surface and circulation $\Gamma \equiv 2\pi vr$ (or angular momentum $M \equiv vr$) is conserved. Inside the core, Γ varies as r^2 (Fig. 1b). From the core wall to radial infinity, $\Gamma = \text{constant} \equiv \Gamma_\infty \equiv 2\pi M_\infty$ (subscript ∞ denotes value at $r = \infty$) because the outer flow is irrotational. The core wall

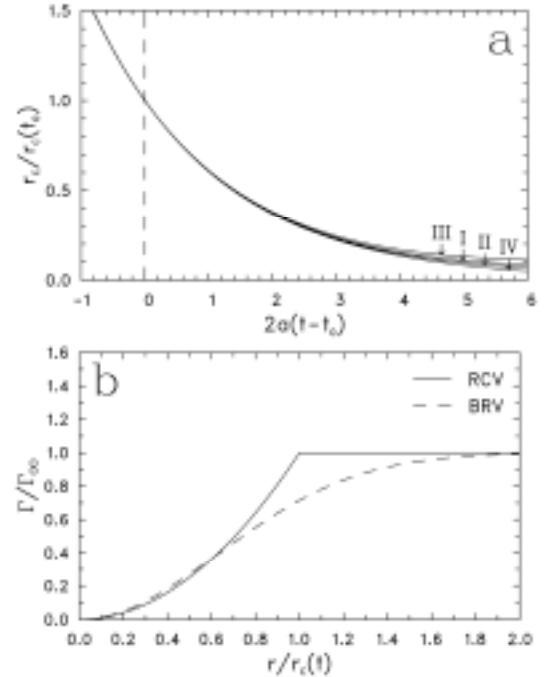


Fig. 1. The unsteady RCV and BRV solutions. (a) Core radius divided by initial core radius as a function of nondimensional time $2a(t-t_0)$ for the RCV of EXP IV and the BRVs of EXP I-III. For $a < 0$, time increases to the left and the core radius increases. There is one curve per value of asymptotic core radius divided by initial core radius. For EXPS I-IV, this ratio is 0.0707, 0.05, 0.1, and 0, respectively. (b) Nondimensional circulation Γ/Γ_∞ in a RCV and a BRV as a function of $r/r_c(t)$.

advects inward (or outward if $a < 0$) with the radial velocity $-ar_c(t)$ (Fig. 2). Since the circulation is constant in the outer region, the maximum tangential velocity at any instant is

$$v_m(t) = M_\infty / r_c(t) = v_m(t_0) \exp[a(t - t_0)]. \quad (4)$$

For fixed $v_m(t_0)$, the time that it takes for the maximum tangential velocity in a RCV to reach a given threshold is inversely proportional to the convergence. The unsteady RCV becomes a line vortex at $t = \infty$ if $a > 0$. The angular velocity of the core is

$$\omega_c(t) = v_m(t) / r_c(t) = [v_m(t_0) / r_c(t_0)] \exp[2a(t - t_0)]. \quad (5)$$

The growth rate of the core rotation is twice that of the maximum tangential velocity.

Rott (1958) found and Trapp and Davies-Jones (1997) used the unsteady BRV (Fig. 2). The solution for tangential

velocity is

$$v(r, t) = (M_\infty / 2\pi) \{1 - \exp[-Kr^2 / r_c^2(t)]\} \quad (6)$$

where $K = 1.2564$ and

$$r_c^2(t) = r_c^2(t_0) \exp[-2a(t - t_0)] + 4Kv_e \{1 - \exp[-2a(t - t_0)]\} / 2a \quad (7)$$

(Fig. 1a). The maximum tangential velocity is

$$v_m(t) = 0.71532 M_\infty / r_c(t). \quad (8)$$

When $a \leq 0$, the solution represents the weakening of an initial vortex owing to viscous diffusion and also vortex spreading in divergent flow (if $a < 0$). Unlike the unsteady RCV, the unsteady BRV in convergent flow approaches a finite steady state asymptotically. When $r_c^2(t_0) \gg r_c^2(\infty)$, the core initially advects inward with little viscous retardation (Fig. 2). Outward diffusion of angular momentum becomes increasingly more important as the vortex contracts and intensifies. The core radius approaches its limiting value when outward diffusion almost balances inward advection of angular momentum. Owing to diffusion, angular momentum is not conserved and the core wall is not a material surface. Nevertheless, the angular momentum at the core wall is an invariant that is equal to $0.71532 M_\infty$ from (8). In fact, the profile of circulation normalized by Γ_∞ is a function of $r/r_c(t)$ alone (Fig. 1b). For the corresponding RCV, (same parameters except $v_e = 0$), the circulation at the core wall is Γ_∞ . Since this RCV has a core radius that is always less than that of the BRV, its maximum tangential velocity is at least 1.398 ($1 / 0.71532$) times that of the BRV.

3. VORTEX FLOWS USED IN THE EXPERIMENTS

We performed five experiments with different flow parameters (see Table 1). In all five experiments, the circulation at radial infinity, Γ_∞ , is $5 \times 10^4 \text{ m}^2 \text{ s}^{-1}$, roughly the value deduced for the 8 June 1953 Cleveland, Ohio tornado (Lewis and Perkins 1953), which was F3 intensity on the Fujita scale (Grazulis 1990). This circulation is small compared to the circulation of a typical mature mesocyclone

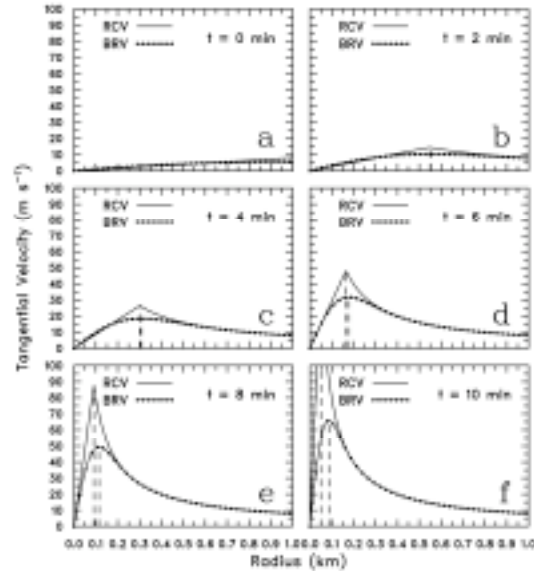


Fig. 2. Evolution of the radial profiles of tangential velocity $v(r, t)$ of the time-dependent BRV in EXP I (dotted curve) and the time-dependent RCV in EXP IV (plain solid curve). Panels a-f show the profiles at 2 min intervals from 0 to 10 min. The maximum wind speed of the RCV at 10 min (off the scale) is 160 m s^{-1} . Vertical dashed lines indicate the core radius (where the maximum tangential wind occurs).

($\sim 4 \times 10^5 \text{ m}^2 \text{ s}^{-1}$), so apparently only a part of a mesocyclone contracts into a tornado. From (1)-(8) it is evident that the results apply for any other circulation at infinity, say $\hat{\Gamma}_\infty$, if the tangential velocities are multiplied by $\hat{\Gamma}_\infty/5 \times 10^4 \text{ m}^2 \text{ s}^{-1}$ (the other variables do not change). In all cases, the initial state may be regarded as a convergent tornado cyclone with an initial core radius of 1 km. The ‘tornadoes’ grow rapidly and form simultaneously at all heights. Thus we are simulating tornadogenesis without a dynamic pipe effect (Trapp and Davies-Jones 1997). We consider our simulated vortices to be tornadoes rather than tornado cyclones when their maximum tangential velocity exceeds the wind-speed threshold for an F1 tornado (33 m s^{-1} according to Fujita 1981). This speed roughly marks the onset of significant damage.

The evolution of the vortices is controlled mainly by the parameters a and $(a/v_e)^{1/2}$. In all the experiments, the core radius advects inward with little retardation at first because the core radius is large initially compared to its asymptotic value. Therefore, the early growth rate of $v_m(t)$ and $r_c^{-1}(t)$ is a , which from (3) and (4) is the constant growth rate of a RCV. The asymptotic values of $v_m(t)$ and $r_c^{-1}(t)$ are proportional to $(a/v_e)^{1/2}$.

We regard Experiment (EXP) I as the control case and the other experiments as deviations from this case. In EXP I, the flow is a time-dependent BRV with an eddy viscosity of $10 \text{ m}^2 \text{ s}^{-1}$ and a horizontal convergence of 10^{-2} s^{-1} . The flow evolves asymptotically towards a steady F3 tornado with maximum tangential velocity $v_m(\infty) = 80 \text{ m s}^{-1}$ and core radius $r_c(\infty) = 71 \text{ m}$ (Figs. 2, 3a). Halving the viscosity (EXP II) results in a stronger [$v_m(\infty) = 114 \text{ m s}^{-1}$] and narrower [$r_c(\infty) = 50 \text{ m}$] tornado that forms as quickly and intensifies to nearly F5 intensity (Fig. 3b). Halving the convergence instead results in a slowly evolving F2 tornado (EXP III) with $v_m(\infty) = 57 \text{ m s}^{-1}$ and $r_c(\infty) = 100 \text{ m}$ (Fig. 3c). The vortex becomes a tornado at 13 min compared to 6 min for EXP I and II and 5 min for EXP IV. In EXP IV, we eliminate viscosity from the control run.

TABLE 1. The five vortex flows (EXP I-V) used in this study. Listed are the vortex type, the eddy viscosity, the convergence, and the time interval of the whole experiment (EXP I-III) or the part of the experiment when the listed convergence is applied (EXP IV-V). The circulation at radial infinity is $5 \times 10^4 \text{ m}^2 \text{ s}^{-1}$ and the initial core radius is 1 km in all the experiments. The last two columns give the asymptotic values (at $t = \infty$) of the maximum tangential velocity and core radius (where applicable).

EXP	Vortex type	v_e (m ² /s)	2a (s ⁻¹)	Time (min)	$V_m(\infty)$ (m/s)	$R_c(\infty)$ (m)
I	BRV	10	.01	[0, 20]	80	71
II	BRV	5	.01	[0, 20]	114	50
III	BRV	10	.005	[0, 20]	57	100
IV	RCV	0	.01	[0, 10]		
		0	-.01	[10, 20]		
V	BRV	10	.01	[0, 20]		
		10	0	[20, 40]		

This produces a RCV that intensifies exponentially during the 10 minutes that the convergence is maintained (Fig. 2, 3d). For the first six min the core radius of the RCV is only slightly smaller than the core radii of the BRVs in EXPs I and II. At 10 min, the maximum tangential velocity is unrealistically high, 160 m s^{-1} . The sign of the convergence is switched at this time to illustrate the effect of a vortex being overtaken by divergent flow. The RCV decays after 10 min at the same rate as it was intensifying during the first 10 min (Fig. 3d). EXP V illustrates the viscous decay of the vortex in the control case (EXP I) when the updraft abruptly dies at 20 min. (Fig. 3e). The vortex at this time has almost reached its asymptotic steady state with a maximum tangential velocity of 80 m s^{-1} . Beyond 20 min the BRV's core radius spreads out according to (7) (with $t_0 = 1200 \text{ s}$ and $a \rightarrow 0$) as angular momentum diffuses outward. Since the angular momentum at the core wall is still an invariant, the maximum tangential velocity is inversely proportional to the core radius. Five minutes after the death of the updraft, the core radius is double its minimum value and the maximum tangential wind is one half of its maximum value. The vortex ceases to be a tornado (according to our arbitrary definition) at 28 min. Exp IV and V may illustrate the decay

of a minority of tornadoes. Most tornadoes narrow and tilt over while decaying as they become susceptible to the action of wind shear (Golden and Purcell 1978). However, a few do seem to decay by spreading outward owing to rapid weakening of the parent updraft (Agee et al. 1976; Davies-Jones et al. 2001; Bluestein et al. 2003).

4. THE DOPPLER VELOCITY FIELDS OF THE VORTEX FLOWS

a. The analytical Doppler-radar simulator

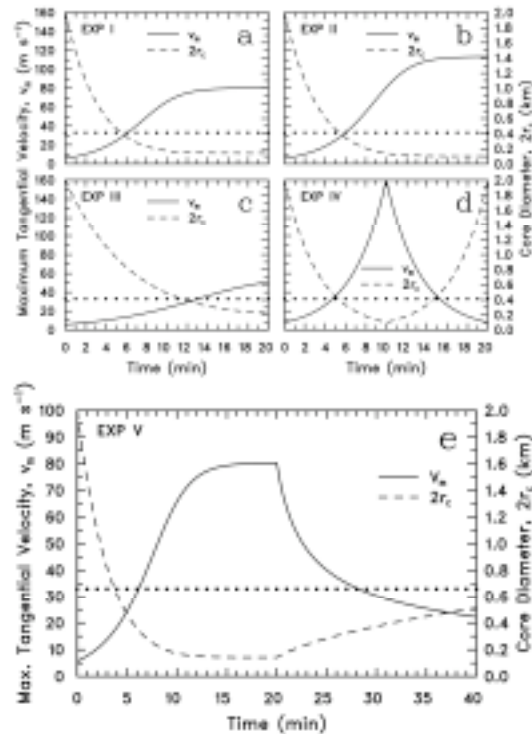


Fig. 3. Maximum tangential velocity $v_m(t)$ (solid curve) and core diameter $2r_c(t)$ (dashed curve) for the BRVs of EXP I-III (panels a-c), the RCV of EXP IV (panel d), and the BRV of EXP V (panel e). In order of experiment, the eddy viscosity is $10 \text{ m}^2 \text{ s}^{-1}$, $5 \text{ m}^2 \text{ s}^{-1}$, $10 \text{ m}^2 \text{ s}^{-1}$, $0 \text{ m}^2 \text{ s}^{-1}$, and $10 \text{ m}^2 \text{ s}^{-1}$. The convergence is 10^{-2} s^{-1} in EXP I and II, and $5 \times 10^{-3} \text{ s}^{-1}$ in EXP III. The convergence switches from 10^{-2} s^{-1} to -10^{-2} s^{-1} at $t = 10 \text{ min}$ in EXP IV, and from 10^{-2} s^{-1} to 0 at $t = 20 \text{ min}$ in EXP V. Note that EXP V is the same as EXP I for the first 20 min. The asymptotic value of v_m in EXP III (panel c) is 56.8 m s^{-1} . Horizontal dotted lines indicate threshold (33 m s^{-1}) for a F1 tornado.

We built an analytical WSR-88D simulator and used it to generate Doppler velocity measurements of the unsteady BRVs and RCVs centered at two different ranges from the Doppler radar. The experiments crudely represent a tornado cyclone shrinking to a tornado as a simulated WSR-88D scans across the developing vortex at the lowest elevation angle, $\theta_0 = 0.5^\circ$. The radar is at 25 or 50 km from the vortex and has a half-power beamwidth, θ_1 , of 0.89° , an half-power effective beamwidth (EBW), ϕ_e , of 1.02° or 1.39° (Wood et al. 2001, Brown et al. 2002), and a pulse width, τ , of $1.57 \times 10^{-6} \text{ s}$ (Doviak and Zrnica 2002, p. 47). We use spherical coordinates (R, θ, ϕ) with origin at the radar where R is slant range, θ is the elevation angle, ϕ is azimuth (measured clockwise from north), and V_R is radial velocity. We denote the point O where the vertical axis of the vortex passes through the θ_0 surface of constant elevation angle by (R_0, θ_0, ϕ_0) . We assume without loss of generality that the vortex is due north of the radar so that $\phi_0 = 0$.

The mean Doppler velocity \bar{V}_R at any point $P \equiv (R_P, \theta_P, \phi_P)$ was found by computing the weighted mean of the Doppler velocity over an effective resolution volume using Gaussian weighting functions (Doviak and Zrnica 1993, p. 118) and assuming uniform reflectivity. The volume is that defined by the -24dB contour surface of the overall weighting function. The volume integrals were performed by the technique described in Press et al. (1986, sections 4.2, 4.6). Winds in (R, θ, ϕ) coordinates were computed as described by Doviak and Zrnica (1993, 306-307). The distance $R_0 \phi_M$ between the axis and the peaks in mean Doppler velocity along $R = R_0$ in the θ_0 surface was found to a tolerance of 1 m by a golden-section search (Press et al. 1986, section 10.1).

b. Simulated Doppler velocity signatures with perfect radar resolution

We start our investigation of the

signatures of the above artificial vortices by computing the Doppler velocity fields for a radar with an infinitesimal beamwidth and pulse width, and hence perfect resolution at all ranges. We assume that the radar measurements are continuous and free of noise. Since the elevation angle is very small, we neglect the contribution to Doppler velocity from the vertical component of scatterer motion. Figures 4-6 show at different times the horizontal winds and the Doppler velocities at 25 km range for the BRV of EXP 1 and the corresponding RCV of EXP IV.

The initial wind fields of the RCV and the BRV are similar (Figs. 4a and c). For the control value of the fixed uniform horizontal convergence (10^{-2} s^{-1}), the radial profile of the radial velocity component (u) decreases linearly from zero at the vortex center to -5 m s^{-1} at the radial distance of 1 km, which initially is the edge of the vortex core. The initial maximum tangential velocity is 8.0 m s^{-1} for a RCV and 5.7 m s^{-1} for a BRV. Inside the solidly rotating core of the RCV, the Doppler-velocity contours are practically straight and parallel (Fig. 4b). This is a consequence of the linear wind field in the core and the large range-core radius ratio, which makes the radar radials in the core region nearly parallel. For nondivergent flow the contours in the core would be parallel to the radar viewing direction. Convergence causes the Doppler velocity patterns of the vortices to rotate in a clockwise direction (Figs. 4b, d; Brown and Wood 1991). Along the range circle $R = R_0$ through the vortex axis (along $y = 25 \text{ km}$ in Fig. 4), the radial inflow of the vortex makes no contribution to the Doppler velocity. Initially there are no peaks in the Doppler-velocity field (Fig. 4) because the tangential wind nowhere dominates the radial wind $u = -ar$. However, in a constrained 1D search along $R = R_0$ we find peak outbound and inbound velocities, which we may regard as a pure-rotation signature (denoted by primes) with a velocity differential $\Delta V'$ (delta- V'), rotational velocity $V'_{\text{rot}} \equiv \Delta V'/2$, and separation distance (or apparent core diameter) D' . Hereafter, 'rotational velocity' refers to V'_{rot} , not V_{rot} . Donaldson and Desrochers (1990 p. 249) found D' and V'_{rot} by a method that works only if u and v have the same dependence on r .

As time progresses (Figs. 5 and 6), the cores contract and the maximum tangential velocities, which are inversely proportional to the core radii, increase rapidly. Flow in and near the vortices becomes more and more tangential as the vortices rotate faster and their inflows remain constant. As a result, the contours of Doppler velocity in the cores become progressively more parallel to the radar viewing direction. By 4 min, each vortex is associated with a Doppler-velocity signature consisting of a couplet of closed contours around peak inbound and outbound Doppler velocities (Fig. 5; Brown and Wood 1991). Owing to convergence, the signature is rotated counterclockwise relative to a pure-rotation signature. However, the rotation part of the signature can still be extracted as before. The signatures contract, intensify, and quickly become oriented in the azimuthal direction as the vortex core spins up (Fig. 6). By 8 minutes (Fig. 6) the couplets have become tornado signatures (Brown et al. 2002). There is now little difference between the convergent-vortex signature and the pure-rotation signature. The simulated Doppler velocity patterns of the BRV evolution, shown in Figs. 5d and 6d, are similar in appearance to the evolution of Doppler velocity signatures of tornadoes (see Fig. 19 of Wakimoto and Wilson 1989, for example). A TVS cannot occur in this case because the simulated radar has perfect azimuthal resolution and samples continuously in azimuth.

c. Simulated Doppler velocity signatures with limited resolution

In the last subsection, we computed the Doppler-velocity fields of the vortices for an ideal radar. We now investigate the effects of limited resolution on the Doppler velocity signatures of the evolving RCV and BRV. Wood et al. (2001) and Brown et al. (2002, 2005) showed that signature resolution of steady Rankine combined mesocyclones and tornadoes is greatly improved (as evidenced by stronger Doppler signatures) when the azimuthal sampling interval, and hence the EBW, is decreased. These signatures are detectable 50% farther in range when azimuthal sampling intervals of 0.5° are used instead of current intervals of 1.0° .

Effective beamwidth accounts for the

broadening of the antenna pattern in the azimuthal direction owing to antenna motion during the time it takes to collect a required number of samples (Zrnica and Doviak 1976, Doviak and Zrnica 1993). The average half-power beamwidth of the operational WSR-88Ds is 0.89° . For the routinely used azimuthal sampling interval of 1.0° the corresponding EBW is 1.39° . This is reduced to 1.02° by decreasing the sampling interval to 0.5° and halving the number of pulses sampled while keeping the same antenna rotation rate (Brown et al. 2002).

We simulated the rotation signatures of the five evolving vortex flows (Table 1) for radar ranges of 25 and 50 km and EBWs of 1.39° and 1.02° . Limiting the search for the peak values to the range

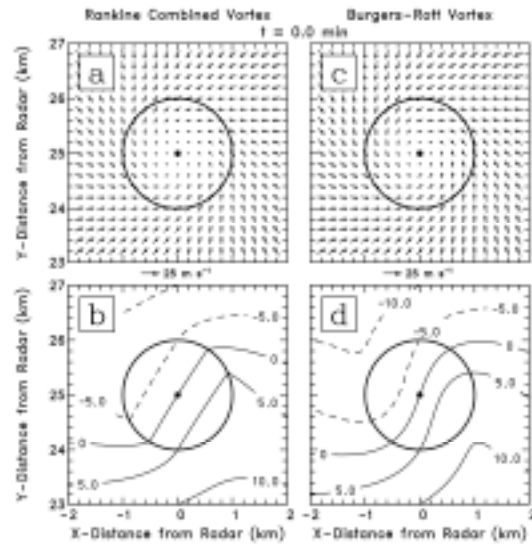


Fig. 4. (a) Horizontal winds of the RCV in EXP IV at $t = 0$ min. (b) Associated contours of Doppler velocity V_R in m s^{-1} for a radar with perfect resolution that is 25 km to south of the RCV. (c) and (d) are same but for the BRV in EXP I. In (a) and (c) wind vector length is proportional to wind speed shown at the bottom of the panel. In (b) and (d) the Doppler velocity is negative (positive) when it is toward (away from) the radar and dashed (solid) Doppler velocity contours represent flow toward (away from) the radar. The zero Doppler-velocity contour (also solid) indicates where the flow is either perpendicular to the radar viewing direction or stagnant. Solid circle and black dot mark the core wall and center of the vortex.

circle $R = R_0$ has the following advantages; the rotation signature is dimensional, the through flow can be excluded without loss, and calculations of signature circulation (defined below) and azimuthal shear are straightforward. The delta- V' and core diameter of a rotation

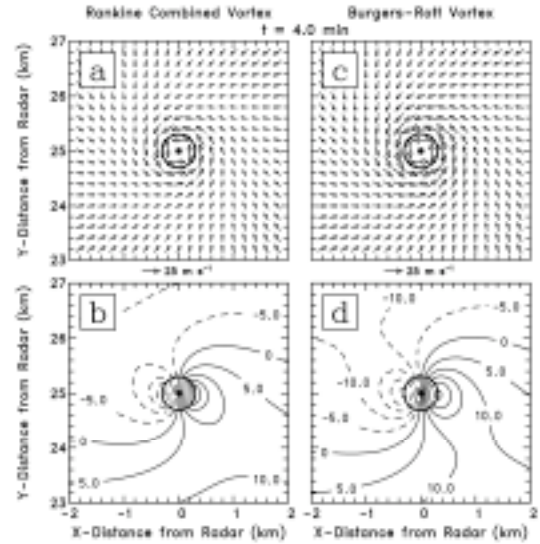


Fig. 5. Same as Fig. 4, except $t = 4$ min.

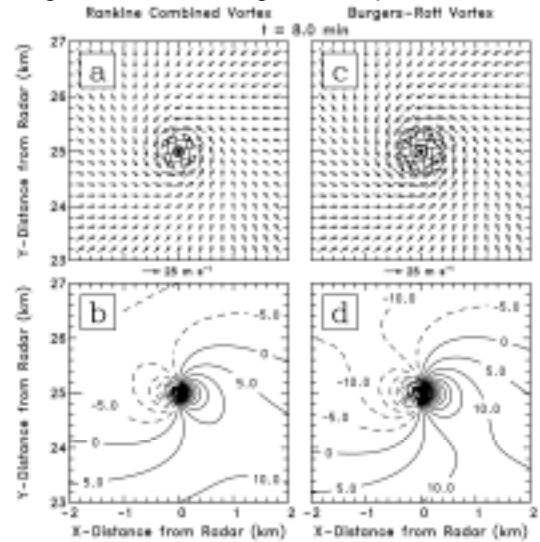


Fig. 6. Same as Fig. 4, except $t = 8$ min.

TABLE 2. Equivalent beam diameters (EBDs) for the equivalent beam widths (EBWs) and radar ranges used in the experiments.

Range (km)	EBW	EBD (m)
25	1.02°	445
25	1.39°	607
50	1.02°	890
50	1.39°	1213

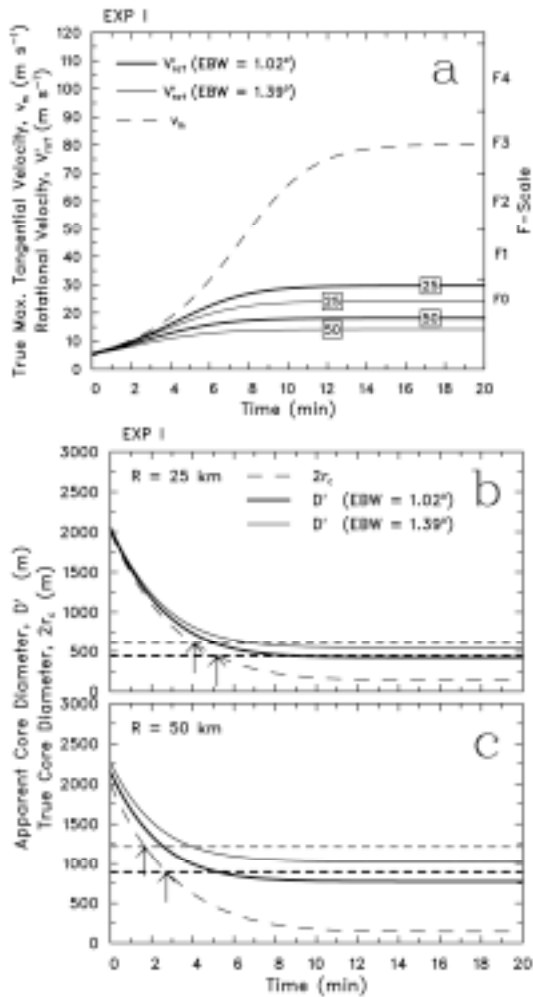


Fig. 7. (a) The time-dependent BRV's maximum tangential velocity $v_m(t)$ (long dashed curve) and its rotational velocity $V'_{rot}(t)$ for EBWs of 1.02° (thick solid curve) and 1.39° (thin solid curve) and ranges of 25 and 50 km from the radar for the control experiment (EXP I). The time interval between data points in this and subsequent figures is 15 s. The F-scale is shown on the right. (b) and (c) same as (a) except that the graphs are of the BRV's core diameter $2r_c(t)$ (long dashed curve) and the apparent core diameter $D'(t)$ of the pure-rotation signature at 25 and 50 km ranges. The horizontal lines mark the effective beam diameters at this range for EBWs of 1.02° (heavy dashed line) and 1.39° (light dashed line). The arrows mark the times when the signature becomes a TVS. The earlier (later) one is for the EBW of 1.39° (1.02°).

signature are calculated here as if the radar were able to make measurements in a continuous manner instead of at discrete points, and so are independent of the location of the vortex axis relative to the center of a sampling volume.

We define the (range-dependent) effective beam diameter (EBD) as the EBW measured in units of distance instead of angle, and compare it to the core diameter of the vortex for the four combinations of range and EBW. The EBDs are listed in Table 2. The EBD is larger for the finer azimuthal resolution at 50 km range than for the coarser resolution at 25 km.

The BRV of EXP I evolves from a broad weak vortex initially to a F3 tornado (Fig. 7). The initial tornado cyclone spins up to a tornado (i.e., to the onset of F1 winds) in 6 min, the time that the 88D takes to perform 1.5 volume scans for VCP 12. At first, the rotational velocity V'_{rot} increases quickly and the apparent core diameter CD'_D decreases rapidly. The signature changes from a tornado-cyclone signature to a tornadic vortex signature (TVS) (see Fig. 7b) as the core diameter becomes smaller than the EBD and the aspect ratio exceeds 2. (Brown et al. 1978, 2002). At a given time, V'_{rot} decreases and D' increases with EBD. Hence, the TVS occurs earlier for larger EBD (Fig. 7). For the EBW of 1.39° (1.02°), the signature becomes a TVS at 1.7 (2.7) min at 50 km range and at 4.1 (5.2) min at 25 km. As the tornado's core diameter becomes smaller than the EBD, the apparent core diameter of the TVS tapers off to a constant value. The rotational velocity levels off as the BRV approaches its asymptotic steady state.

As expected (Brown et al. 2002), the Doppler signature is stronger, tighter and has a larger shear value for the smaller EBW. Another advantage of a smaller EBW is that the signature exceeds a given threshold value of rotational velocity or shear *earlier*. These findings imply that the smaller EBW can improve the lead time of tornado warnings and can result in better detection of weak tornadoes.

In EXP II, the vortex intensifies initially at the same rate as in EXP I but becomes a nearly F5 tornado with a smaller core radius (see Table 1). The differences in the two flows occur primarily after the

signatures have become TVSSs. Consequently, the evolving signatures are almost identical to those of EXP I. At 25 km or greater range, the WSR-88D cannot detect the large difference in tornado intensity between EXP II and EXP I.

The tornado in EXP III (Fig. 3c) is broader, weaker (F2), and takes a longer time to form than the one in EXP I (Fig. 3a). The tornado begins at 13 min and the signatures for 1.39° (1.02°) EBW become TVSSs at 3.4 (5.5) min at 50 km range and at 8.3 (10.7) min at 25 km. This is the case with the longest lead times between TVS and tornado formation. The apparent core diameters and rotational velocities at the time of tornado formation are about the same as in EXPs I and II.

For the first ten min, EXP IV is the same as EXP I, except there is no diffusion and the vortex is a RCV instead of a BRV. For the first 5-6 min, the core radius is only slightly less than in EXPs I and II (Fig. 1a). Therefore, the tornado-cyclone signatures change to TVSSs at practically the same times as in EXPs I and II. At 8.8 min, the RCV has the same core radius, 71 m, as the asymptotic BRV, and so has a 40% higher maximum tangential velocity (section 2b). As the RCV continues to contract and intensify without limit, the apparent core diameter levels off but the rotational velocity continues to amplify slowly owing to higher winds in the narrowing velocity peaks (Fig. 2). At 10 min the RCV's maximum tangential winds reach double (160 m s⁻¹) those for the asymptotic BRV, but the rotational velocities are only slightly higher than in EXP I. At this time, the convergence is switched to divergence of the same magnitude, resulting in curves that are symmetric about the $t = 10$ min line.

EXP V is the same as EXP I except that the parent updraft is "switched off" at $t = 20$ min and the vortex diffuses outward thereafter. From 20 to 28.2 min, the actual maximum winds fall from 80 to 33 m s⁻¹ (our threshold value for a tornado) but the Doppler rotational velocities for the smallest EBD (445 m; see Table 2) only decrease from 30 m s⁻¹ to 23 m s⁻¹ as the true core radius increases from 71 m to 172 m. For all four EBDs, the apparent core diameter increases far more slowly than the actual diameter. At 25 km range with the 1.02° EBW, the signature ceases

to be a TVS at 35 min. For the three larger EBDs in Table 2, the TVS persists until well after 40 min.

5. CIRCULATION, SHEAR AND ERKE OF DOPPLER SIGNATURE

Davies-Jones and Stumpf (1997) advocated using detection of significant circulation around a material curve that is contracting as a method for giving advance warnings of tornadoes. Circulation is the basic measure of macroscopic rotation in a fluid. The circulation around a closed curve C is

$$\Gamma = \oint_C \mathbf{v} \cdot d\mathbf{s}, \quad (9)$$

where $d\mathbf{s}$ is an element of C and \mathbf{v} is the wind vector. In the RCV, circulations around material horizontal circles are conserved. Using WSR-88D data, Davies-Jones and Stumpf estimated the circulations and areal expansion rates around circles centered on signatures. Here, we define the circulation of a Doppler rotation signature as $\Gamma_D \equiv \pi D' \Delta V' / 2$. This is the measured circulation around the apparent core circumference. It resembles the momentum parameter $D\Delta V$ (Zrnich et al. 1985), which additionally includes effects of areal expansion rate.

The Doppler circulation of a vortex depends on the aspect ratio $AR \equiv EBD/r_c(t)$. The AR ranges from .44 to 1.22 initially for the adopted ranges and EBWs, and eventually exceeds 4 during vortex contraction in all the experiments. Consider first how the Doppler circulation of the RCV evolves. The actual circulation at the core wall of a RCV is Γ_∞ . Initially, the core of the RCV is well resolved, but the cusp in the velocity profile at the core wall is smoothed owing to the Doppler velocities being weighted means over sampling volumes. Therefore, the core radius is quite accurately measured (Fig. 4b), but the observed peak velocity is undervalued (Burgess et al. 1993 Fig. 3; Wood and Brown 1997, p. 931). Thus Γ_D underestimates Γ_∞ at $t=0$ by amounts that increase with EBD (Fig. 8a). While the contracting vortex is still broad, the core diameter D' remains well estimated. However, $\Delta V'$ does not increase as fast as v_m because the growing peak in the

velocity profile becomes more pointed and so is reduced to a relatively greater extent by the averaging (Burgess et al. 1993 Fig. 3). Therefore, Γ_D decreases at first. As the vortex contracts further, the EBDs become much larger than the core diameter. The largest $\Delta V'$ occurs when the tornado is centered between range bins at the same range (Fig. 1 of Brown

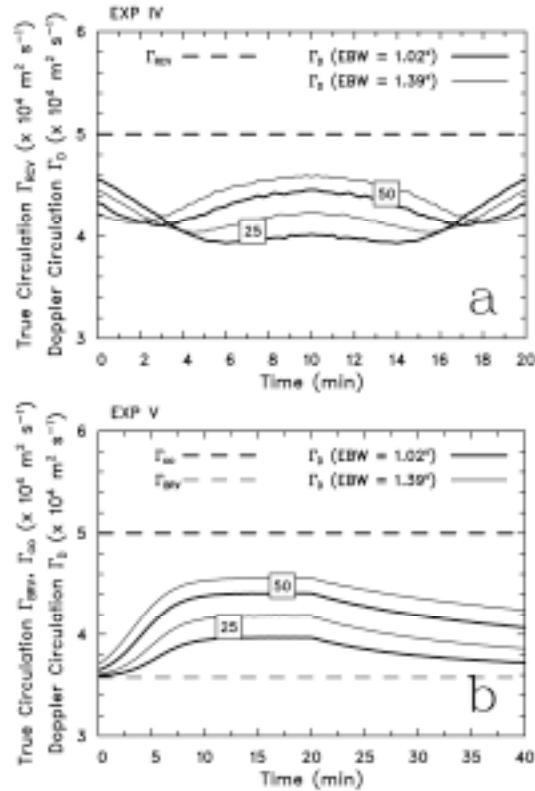


Fig. 8. Circulation of the Doppler signature $\Gamma_D(t)$ for EBWs of 1.02° (heavy solid curve) and 1.39° (light solid curve) and ranges of 25 and 50 km from the radar (a) for EXP IV, and (b) for EXP I (first 20 min only) and EXP V (full 40 min). In (a), the wiggles in the curves expose the limitations of the numerical procedures when the computations are performed with single precision and the velocity profile has a cusp. The heavy dashed line in (a) shows the circulation Γ_{RCV} of the RCV outside the core. The heavy and light horizontal dashed lines in (b) indicate the circulation of the BRV at radial infinity (Γ_∞) and at the radius of maximum winds (Γ_{BRV}), respectively. The true circulation outside the core increases with radial distance from Γ_{BRV} to Γ_∞ as in Fig. 1b.

1998). This tornado location is realized in our simulation because we have assumed that the radar is able to make measurements in a continuous manner across the vortex. For this tornado position, the Doppler velocity peaks are located well outside the core and are good estimates of the actual velocity at their locations. Hence, the Doppler circulation now increases towards Γ_∞ as the aspect ratio increases (Fig. 8a).

In EXP I, the vortex is a BRV instead of a RCV. In a BRV, the actual circulation at the core wall is $0.71532\Gamma_\infty$ and the tangential-velocity peak is rounded instead of cusp-shaped. Initially, the core is well resolved and the peak velocity is not undervalued much because the maximum is broad (Sullivan 1959 Fig. 2). Thus $\Gamma_D \approx 0.71532\Gamma_\infty$ (Fig. 8b). When the core becomes small compared to the EBD, the Doppler velocity peaks move away from the core wall to radii where the circulation is nearly Γ_∞ . Consequently, Γ_D moves closer to Γ_∞ from below as the core contracts. Figure 8b for EXPs I and V and similar figures (not shown) for EXP II and III, confirm these deductions by illustrating that (i) Γ_D increases from near $0.71532\Gamma_\infty$ ($35,766 \text{ m}^2 \text{ s}^{-1}$) to an asymptotic value (that increases with EBD) below Γ_∞ ($50,000 \text{ m}^2 \text{ s}^{-1}$) as the vortex contracts from tornado cyclone to tornado, and (ii) the Doppler circulations of the BRVs increase with EBD (listed in Table 2). We now compare the BRV in EXP I with the corresponding convergent RCV (present during the first 10 min of EXP IV). Since the RCV has a 40% larger circulation at the core wall owing to the cusp in its tangential-velocity profile and a slightly smaller apparent core diameter, the RCV signature has the larger rotational velocity and the larger Doppler circulation (c.f. Figs. 8a, b). The difference in the Doppler circulations decreases as the aspect ratio becomes large and the region where the two vortices differ significantly (Fig. 1b) becomes small compared to the resolution volume.

All through the evolution of the vortex signature from tornado cyclone to TVS (and vice-versa in EXPs IV and V), the Doppler measurements reproduce the circulation quite well. Unlike other parameters such as ΔV and shear S_D ,

Doppler circulation of a signature always gives a fairly good estimate of the actual parameter and is relatively insensitive to range, beamwidth, and vortex evolution even after the signature becomes a TVS. The momentum parameter also has little or no dependence on range (Zrnica et al. 1985). Since momentum is fairly similar to circulation, this observational finding is consistent with our results. The circulation is high throughout the 6 min prior to tornado formation in EXP I and so a large value would be measured at low levels at least once by the WSR-88D (which takes 4 min to perform one volume scan). In contrast, high values of ΔV might go undetected because ΔV increases rapidly during tornadogenesis (Fig. 7a). A large Doppler circulation in convergent flow may provide early warning of imminent tornadogenesis before ΔV becomes large.

Shear, an additional parameter used in tornado detection algorithms (Mitchell et al. 1998), seems to be an even poorer warning parameter than ΔV . As predicted by (5), shear grows very rapidly as vortex core contracts (Fig. 9) and its winds intensify, it is highly dependent on range and the EBW (Fig. 9), and it grossly underestimates the actual value. Another tornado predictor is the excess rotational kinetic energy (ERKE; Donaldson and Desrochers 1990). The rotational

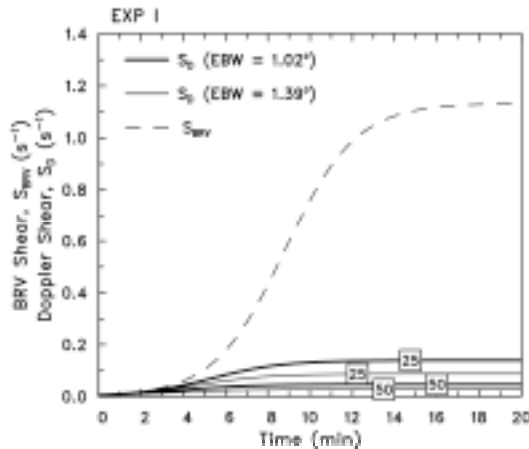


Fig. 9. Actual and measured shear parameters versus time for the BRV of EXP I. S_{BRV} is defined as $v_m(t)/r_c(t)$. The corresponding quantity for a Doppler rotation signature is $S_D \equiv \Delta V'/D'$. This is plotted for EBWs of 1.02° and 1.39° and ranges of 25 and 50 km.

kinetic energy (RKE) is proportional to Γ_D^2 , and so is similar to, but more variable than, Γ_D . The ERKE is the RKE calculated with a Doppler circulation diminished by subtracting $\pi D'^2 S_m/2$ (the circulation of the 'threshold mesocyclone' with the same radius) where S_m is the threshold value of shear for a mesocyclone ($S_m = 0.005 \text{ s}^{-1}$). If the resulting circulation is negative, the ERKE is set to zero, which is the minimum value possible. Unfortunately, the ERKE of the initial tornado cyclone is zero in our experiments (Fig. 10). This would cause a loss in lead time of a warning based on the ERKE in lieu of RKE or Γ_D . Incidentally, the ERKE does not vary monotonically with EBD (Fig. 10) because the Doppler circulations of the BRV (Fig. 12b) and the 'threshold mesocyclone' both increase with EBD.

6. CONCLUSIONS

Our simulated Doppler measurements of evolving Burgers-Rott and Rankine combined vortices show how Doppler velocity signatures of the vortices vary during various stages of tornado evolution. The results apply to tornadoes that form without a dynamic pipe effect. We obtain different vortices by changing the values of convergence and eddy viscosity, while keeping the circulation at infinity fixed. The main conclusions of this study are:

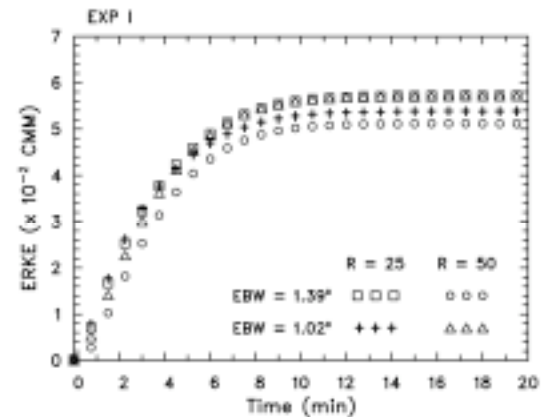


Fig. 10. Time variation of ERKE for the BRV of EXP I for EBWs of 1.02° and 1.39° and ranges of 25 and 50 km. ERKE is in CMM units (i.e., it is normalized by the ERKE value for the Climatological Mature Mesocyclone -- Donaldson and Desrochers 1990). The tornado forms at 6 min.

1. Simulating signatures of exact time-dependent vortex solutions provides a good means of deducing the behavior of tornado predictors as tornado cyclones contract to tornadoes.
2. In convergent flow, the RCV intensifies exponentially as its core radius decreases exponentially and it becomes a line vortex in infinite time. The corresponding BRV also amplifies but approaches a steady state asymptotically as a balance is approached between inward advection and outward diffusion of angular momentum. The growth rate for maximum tangential velocity of the time-dependent RCV is a (one half of the uniform convergence). This is also the initial growth rate of the BRV if the initial core radius is large compared to the asymptotic value.
3. The theoretical solutions indicate that tornadoes can develop from tornado cyclones in about six minutes if they are the type that form without a dynamic pipe effect. This is only slightly larger than the time that the WSR-88D takes to complete one volume scan so the lead time of warnings depends on where the WSR-88D is in its scanning cycle during tornadogenesis.
4. With decreasing EBD, the Doppler-velocity signature of a given vortex is stronger, the apparent core diameter is smaller, and the measured shear is larger. ΔV thresholds are exceeded earlier and the tornado-cyclone signature changes into a TVS later.
5. For the same convergence and EBD, halving the eddy viscosity produces a much stronger tornado, but hardly changes the early growth rate and the TVS. The increase in tornado intensity is practically invisible to the WSR-88D.
6. Halving the convergence instead of the eddy viscosity results in a weaker, broader tornado that forms more slowly and increases the lead time that would be provided by tornado detection algorithms.
7. In contrast to parameters such as ΔV and especially shear, the circulation of a Doppler-velocity signature provides a fairly good estimate of the actual value for the vortex, and is relatively insensitive to range, beamwidth, and stage of vortex evolution. Circulation in combination with convergence may provide an early indication of tornadogenesis.

8. The tornado predictor, ERKE, increases rapidly from zero as the initial tornado cyclone contracts to a tornado and so does not provide much advance warning.

Acknowledgments. The authors thank Mr. Don Burgess, Dr. Dusan Zrnica and Dr. Rodger Brown of NSSL for helpful comments. Dr. Zrnica also provided the Gaussian weighting functions for the simulator. The computations were performed on a Power Mac G5 using FORTRAN code containing copyrighted subprograms from Numerical Recipes Software 1986. [Mention of commercial products does not constitute endorsements by NOAA.] The lead author's work was supported in part by NSF grant ATM-00340693.

7. REFERENCES

- Agee, E. M., J. T. Snow, and P. R. Clare, 1976: Multiple vortex features in the tornado cyclone and the occurrence of tornado families. *Mon. Wea. Rev.*, **104**, 552-563.
- Bluestein, H. B., W.-C. Lee, M. Bell, C. C. Weiss, and A. L. Pazmany, 2003: Mobile Doppler radar observations of a tornado in a supercell near Bassett, Nebraska, on 5 June 1999. Part II: Tornado-vortex structure. *Mon. Wea. Rev.*, **131**, 2968-2984.
- Brown, R. A., 1998: Nomogram for aiding the interpretation of tornadic vortex signatures measured by Doppler radar. *Wea. Forecasting*, **13**, 505-512.
- _____, and V. T. Wood, 1991: On the interpretation of single-Doppler velocity patterns within severe thunderstorms. *Wea. Forecasting*, **6**, 32-48.
- _____, D. W. Burgess, and L. R. Lemon, 1978: Tornado detection by pulsed Doppler radar. *Mon. Wea. Rev.*, **106**, 29-38.
- _____, V. T. Wood, and D. Sirmans, 2002: Improved tornado detection using simulated and actual WSR-88D data with enhanced resolution. *J. Atmos. Oceanic Technol.*, **19**, 1759-1771.
- _____, B. A. Flickinger, E. Forren, D. M. Schultz, D. Sirmans, P. L. Spencer, V. T. Wood, and C. L. Ziegler,

- 2005: Improved detection of severe storms using experimental high-resolution WSR-88D measurements. *Wea. Forecasting*, **20**, 3-14.
- Burgers, J. M., 1948: A mathematical model illustrating the theory of turbulence. *Adv. Appl. Mech.*, **1**, 197-199.
- Burgess, D. W., 2004: High-resolution analyses of the 8 May 2003 Oklahoma City storm. Part I: Storm structure and evolution from radar data. *Preprints*, 22nd Conf. Severe Local Storms, Hyannis, MA, Amer. Meteor. Soc., CD-ROM, 12.4.
- _____, R. J. Donaldson, Jr., and P. R. Desrochers, 1993: Tornado detection and warning by radar. *The Tornado: Its Structure, Dynamics, Prediction, and Hazards, Geophys. Monogr.*, No. 79, Amer. Geophys. Union, 203-211.
- _____, M. A. Magsig, J. Wurman D. C. Dowell, and Y. Richardson, 2002: Radar observations of the 3 May 1999 Oklahoma City tornado. *Wea. Forecasting*, **17**, 456-471.
- Davies-Jones, R. P., and G. J. Stumpf, 1997: On the detection and measurement of circulation and areal expansion rate with WSR-88D radars. *Preprints*, 28th Conf. on Radar Meteorology, Austin, TX, Amer. Meteor. Soc., 313-314.
- _____, R. J. Trapp, and H. B. Bluestein, 2001: Tornadoes and tornadic storms. *Severe Convective Storms, Meteor. Monogr.*, No. 50, Amer. Meteor. Soc., 167-221.
- Donaldson, R. J., Jr. and P. R. Desrochers, 1990: Improvement of tornado warnings by Doppler radar measurement of mesocyclone rotational kinetic energy. *Wea. Forecasting*, **5**, 247-258.
- Doviak, R. J., and D. S. Zrnich, 1993: *Doppler Radar and Weather Observations*. 2nd Ed. Academic Press, 562 pp.
- Fujita, T. T., 1981: Tornadoes and downbursts in the context of generalized planetary scales. *J. Atmos. Sci.*, **38**, 1511-1534.
- Golden, J. H., and D. Purcell, 1978: Life cycle of the Union City, Oklahoma tornado and comparison with waterspouts. *Mon. Wea. Rev.*, **106**, 3-11.
- Grazulis, T. P., 1990; *Significant tornadoes 1880-1989. Volume II: A Chronology of Events*. Environmental Films, St Johnsbury, VT, 685 pp. [ISBN 1-879362-02-3]
- Lewis, W., and P. J. Perkins, 1953: Recorded pressure distribution in the outer portion of a tornado vortex. *Mon. Wea. Rev.*, **81**, 379-385.
- Mitchell, E. D., S. V. Vasiloff, G. J. Stumpf, A. Witt, M. D. Eilts, J. T. Johnson, and K. W. Thomas, 1998: The National Severe Storms Laboratory Tornado Detection Algorithm. *Wea. Forecasting*, **13**, 352-366.
- Press, W. H., B. P. Flannery, S. A. Teukolsky, and W. T. Vetterling, 1986: *Numerical Recipes: The Art of Scientific Computing*. Cambridge University Press, 818 pp.
- Rankine, W. J. M., 1901: *A Manual of Applied Mechanics*. 16th ed. Charles Griff and Co., 680 pp.
- Rott, N., 1958: On the viscous core of a line vortex. *Z. Angew. Math. Physik*, **96**, 543-553.
- Stumpf, G. J. A. Witt, E. D. Mitchell, P. L. Spencer, J. T. Johnson, M. D. Eilts, K. W. Thomas, and D. W. Burgess, 1998: The National Severe Storms Mesocyclone Detection Algorithm for the WSR-88D. *Wea. Forecasting*, **13**, 304-326.
- Sullivan, R. D., 1959: A two-cell vortex solution of the Navier-Stokes equations. *J. Aerospace Sci.*, **26**, 767-768.
- Trapp, R. J., and R. Davies-Jones, 1997: Tornadogenesis with and without a dynamic pipe effect. *J. Atmos. Sci.*, **54**, 113-133.
- Wakimoto, R. M., and J. W. Wilson, 1989: Non-supercell tornadoes. *Mon. Wea. Rev.*, **117**, 1113-1140.
- _____, H. V. Murphey, D. C. Dowell, and H. B. Bluestein, 2003: The Kellerville tornado during VORTEX: Damage survey and Doppler radar analyses. *Mon. Wea. Rev.*, **131**, 2197-2221.
- Wood, V. T., and R. A. Brown, 1992: Effects of radar proximity on single-Doppler velocity signatures of axisymmetric rotation and divergence. *Mon. Wea. Rev.*, **120**, 2798-2807.
- _____, and _____, 1997: Effects of radar sampling on single-Doppler velocity signatures of

mesocyclones and tornadoes. *Wea. Forecasting*, **12**, 928-938.

_____, _____, and D. Sirmans, 2001: Technique for improving detection of WSR-88D mesocyclone signatures by increasing angular sampling. *Wea. Forecasting*, **16**, 177-184.

Zrnich, D. S., and R. J. Doviak, 1976: Effective antenna pattern of scanning radars. *IEEE Trans. Aerospace Electron. Systems*, **AES-12**, 551-555.

_____, D. W. Burgess, and L. D. Hennington, 1985: Automatic detection of mesocyclonic shear with Doppler radar. *J. Atmos. Oceanic Technol.*, **2**, 425-438.